Glide symmetry breaking and Ising criticality in the quasi-1D magnet $CoNb_2O_6$

Michele Fava[a], Radu Coldea[b], and S. A. Parameswaran[a,1]

[a]Rudolf Peierls Centre for Theoretical Physics, Department of Physics, University of Oxford, Oxford OX1 3PU, United Kingdom; and [b]Clarendon Laboratory, Department of Physics, University of Oxford, Oxford OX1 3PU, United Kingdom

Edited by Subir Sachdev, Harvard University, Cambridge, MA, and approved August 18, 2020 (received for review May 19, 2020)

We construct a microscopic spin-exchange Hamiltonian for the quasi–one-dimensional (1D) Ising magnet $CoNb_2O_6$ that captures detailed and hitherto-unexplained aspects of its dynamic spin structure factor. We perform a symmetry analysis that recalls that an individual Ising chain in this material is buckled, with two sites in each unit cell related by a glide symmetry. Combining this with numerical simulations benchmarked against neutron scattering experiments, we argue that the single-chain Hamiltonian contains a staggered spin-exchange term. We further argue that the transverse-field–tuned quantum critical point in $CoNb_2O_6$ corresponds to breaking this glide symmetry, rather than an on-site Ising symmetry as previously believed. This gives a unified microscopic explanation of the dispersion of confined states in the ordered phase and quasiparticle breakdown in the polarized phase at high transverse field.

quasi-1D magnets | Ising chain | nonsymmorphic symmetries

Magnetic materials with a large mismatch of exchange strengths along different crystalline axes can often be understood from a one-dimensional (1D) starting point. In this paper, we focus on a celebrated example of such a quasi-1D magnet (1), $CoNb_2O_6$ (2–5), usually viewed as a system of weakly coupled ferromagnetic Ising chains (6). Several theoretical predictions rooted in this perspective that leverage techniques ranging from integrability and conformal field theory (CFT) (7–11) to matrix-product state numerical methods (12) have been verified via neutron scattering experiments. Especially striking among these are studies of the transverse-field–tuned quantum critical point (QCP) (13–16), considered a canonical example of the Ising universality class (17). However, many detailed experimental features have resisted a fully microscopic explanation. This is particularly true away from the critical regime, where perturbations to the simplest Ising description play a significant role.

Here we revisit the models used to describe $CoNb_2O_6$, paying attention to the fact that it is only a quasi-1D system. We use a combination of symmetry analysis, time-dependent density-matrix renormalization group (tDMRG) simulations, and exact diagonalization studies to construct a microscopic 1D model, compute its dynamical spin structure factor (DSF), and compare against that measured by inelastic neutron scattering (INS) experiments. By exploring various symmetry-allowed exchange terms beyond the dominant Ising coupling, we find that the origin of various hitherto-unexplained features of the DSF may be traced to a single previously ignored contribution: namely, a staggered nearest-neighbor exchange between y- and z-axis spin components (z is the Ising axis). Its admissibility originates in a subtle and oft-overlooked feature of $CoNb_2O_6$, namely, that the magnetic Co^{2+} ions are arranged in zigzag chains oriented along the c axis as shown in Fig 1*A*, with the primitive unit cell for one chain containing two Co^{2+} sites with staggered displacements along the b axis. In other words, it relies on the fact that the chain is embedded in a 3D crystal, leading to distinct symmetry considerations than in pure 1D. We show that this term controls both 1) the dispersion of confined bound states of two domain wall (DW) excitations (12, 18, 19) in the spontaneously ordered phase for zero and weak transverse fields, previously only captured phenomenologically, and 2) quasi-particle (QP) breakdown, a phenomenon observed (20) in the opposite limit when a strong transverse field drives the system into a polarized quantum paramagnet.

The staggered coupling we consider explicitly breaks both Ising and translational symmetry. Nevertheless, we show that it may be reconciled both with the host of results predicated on the existence of an Ising QCP in $CoNb_2O_6$ and with the absence of Brillouin zone (BZ) halving in the DSF throughout the field-polarized phase. This is because the chain retains a glide symmetry composed of translation by half a lattice spacing ($\tilde{c} = c/2$ in Fig. 1*A*) combined with a reflection; the ordered phase breaks this symmetry. A unitary transformation maps the symmetries of our model to those of an Ising antiferromagnet in a transverse field and the glide-breaking transition to the breaking of discrete translational symmetry in that model, known to be in the Ising universality class (21–23). The transformed Hamiltonian has a single-site unit cell, and the transformation effectively unfolds the BZ probed by DSF into one twice as large (size $4\pi/c$)—i.e., the same as that observed in experiments. Unit cell doubling is manifest in the DSF only upon breaking the glide symmetry, allowing scattering to directly probe the

Significance

The quasi-1D magnetic insulator $CoNb_2O_6$ hosts a paradigmatic example of a quantum phase transition in the 1D Ising universality class. While the physics near the transition is largely insensitive to the microscopic Hamiltonian, several features observed in neutron-scattering experiments have hitherto remained unexplained. We propose a microscopic Hamiltonian that reproduces the entirety of the experimental phenomenology. This is based on a symmetry analysis of the material where a glide symmetry (translation composed with reflection) plays a crucial role. Strikingly, this sheds light on the microscopic mechanism of the transition itself, linking the Ising order to the breaking of both magnetic and spatial symmetries. We lay the groundwork for future high-precision investigations of Ising criticality, quasiparticle confinement, and quasiparticle decay in a quantum material.

Author contributions: M.F., R.C., and S.A.P. conceived the project; M.F., R.C., and S.A.P. designed research; M.F., R.C., and S.A.P. performed research; M.F., R.C., and S.A.P. analyzed data; M.F. and S.A.P. designed theoretical model and symmetry analysis and performed numerical simulations; R.C. analyzed experimental neutron scattering data and performed the analysis of symmetry-allowed spin-exchange coupling; and M.F., R.C., and S.A.P. wrote the paper.

The authors declare no conflict of interest.

This article is a PNAS Direct Submission.

[1]To whom correspondence may be addressed. Email: sid.parameswaran@physics.ox.ac.uk.

This article contains supporting information online at https://www.pnas.org/lookup/suppl/doi:10.1073/pnas.2007986117/-/DCSupplemental.

First published September 25, 2020.

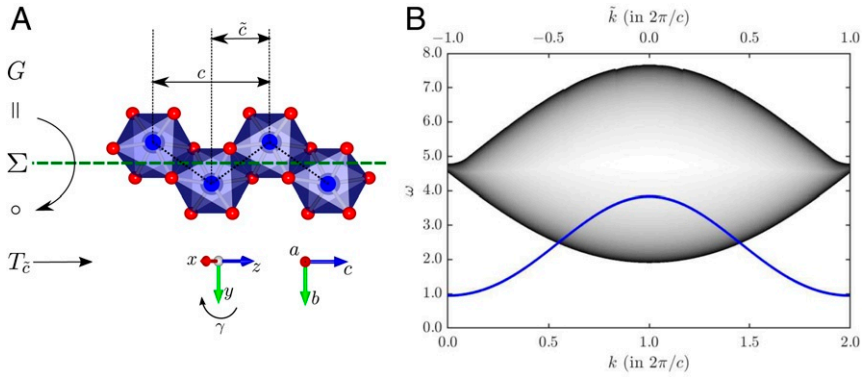

Fig. 1. (*A*) Individual Ising chain in $CoNb_2O_6$. The zigzag structure gives rise to a glide reflection symmetry, corresponding to an *ac*-plane reflection Σ followed by a half-lattice translation $T_{\tilde{c}} = T_{c/2}$. (*B*) Excitation spectrum in the transverse-field polarized quantum paramagnetic phase, showing the band of single spin-flip QPs (blue solid line) and the 2QP continuum (shaded region; darker shading indicates higher density of states). The *x* axis shows both momentum k (bottom) and glide eigenvalue $\tilde{k}$ (top). The position of the 2QP continuum relative to the 1QP band is controlled by conservation of $\tilde{k}$, rather than k, as detailed in the *Quasiparticle Breakdown* section.

glide-breaking order parameter. We show that glide symmetry provides a natural kinematic interpretation of quasiparticle breakdown in the high-field-polarized phase: the decay processes that drive it are constrained by glide selection rules rather than by momentum conservation. This scenario provides a natural explanation of several important features of experimental INS data. Our work gives a fully microscopic understanding of Ising criticality, confinement, and QP breakdown in $CoNb_2O_6$, providing a platform for further studies, and illustrates the subtle interplay of spatial and on-site symmetries in chain and layer compounds with nonsymmorphic space groups.

Symmetries and Microscopic Hamiltonian

In $CoNb_2O_6$, Co^{2+} ions hosting pseudospin-1/2 moments are arranged in zigzag chains along the c axis, with a dominant ferromagnetic Ising coupling along the chain. The chains form a triangular lattice in the ab plane, with nearest-neighbor chains weakly coupled antiferromagnetically. The 3D space group is $Pbcn$ (space group no. 60 in the nomenclature of ref. 24), which includes a glide plane that intersects each chain perpendicular to its zigzag plane (ac plane in Fig. 1*A*). Henceforth, we focus on a single chain and denote by S_j^α the α-component of the spin operator acting on the jth site (even and odd sites lie on different sublattices), with $\alpha \in \{x, y, z\}$, defined as in Fig. 1*A*. The Ising axis z lies in the ac plane at an angle $\gamma = 29.6^\circ$ to c (3), while b is parallel to y.

We propose that the 1D physics in $CoNb_2O_6$ is well captured by the minimal single-chain Hamiltonian

$$\mathcal{H} = J \sum_j \left[-S_j^z S_{j+1}^z + \lambda_{\mathrm{AF}} S_j^z S_{j+2}^z + h_y S_j^y - \lambda_S \left(S_j^x S_{j+1}^x + S_j^y S_{j+1}^y \right) - h_z S_j^z \right] + \mathcal{H}_{dw}. \qquad [1]$$

This includes, apart from the leading nearest-neighbor ferromagnetic Ising exchange coupling, a next-nearest neighbor antiferromagnetic λ_{AF} term (12, 20) as well as an effective longitudinal field $Jh_z = J_{\mathrm{ic}}^{zz} \sum_j \langle S_j^z \rangle / L$ accounting for interchain coupling (parameterized by J_{ic}^{zz}) at the mean-field level. Both of these (as well as λ_S) are needed to reproduce details of the experimental zero-field DSF (18). We also include a transverse field $Jh_y = g_b \mu_B B$, where B is an external magnetic field. All terms in Eq. **1** have been previously identified, except for the final term $\mathcal{H}_{dw}$, which is required to give dynamics to DWs when $h_y = 0$; since its magnitude (12, 18) is much larger than that of interchain couplings [which are $\sim h_z$ (25)], it cannot arise primarily from these. A key goal of this work is to identify a microscopic origin for this DW hopping, which was previously only modeled phenomenologically (12).

To identify $\mathcal{H}_{dw}$, we focus on nearest-neighbor couplings, which are likely dominant, and use a symmetry analysis to narrow our search. Recalling that each unit cell has two magnetic sites (per chain), the nearest-neighbor exchange Hamiltonian takes the form

$$\mathcal{H}_{\mathrm{nn}} = \sum_j \sum_{\alpha,\beta} \mathcal{J}_{\alpha,\beta}^{(1)} S_{2j}^\alpha S_{2j+1}^\beta + \mathcal{J}_{\alpha,\beta}^{(2)} S_{2j+1}^\alpha S_{2j+2}^\beta. \qquad [2]$$

Crystal symmetry further constrains $\mathcal{J}_{\alpha,\beta}^{(n)}$. Inversion about the midpoint between consecutive spins requires $\mathcal{J}_{\alpha,\beta}^{(n)} = \mathcal{J}_{\beta,\alpha}^{(n)}$, while the glide symmetry imposes

$$\mathcal{J}_{\alpha,\beta}^{(1)} = \begin{cases} -\mathcal{J}_{\alpha,\beta}^{(2)} & \text{if } \beta = y \neq \alpha, \\ \mathcal{J}_{\alpha,\beta}^{(2)} & \text{otherwise.} \end{cases} \qquad [3]$$

The most general exchange tensor satisfying these conditions may be parametrized (in the xyz basis) as

$$\mathcal{J}^{(m)} = J \begin{pmatrix} \lambda_S + \lambda_A & (-1)^m \lambda_{xy} & \lambda_{xz} \\ (-1)^m \lambda_{xy} & \lambda_S - \lambda_A & (-1)^m \lambda_{yz} \\ \lambda_{xz} & (-1)^m \lambda_{yz} & -1 \end{pmatrix} \qquad [4]$$

with $m = 1, 2$ and $J > 0$. Taking z along the Ising axis sets $\lambda_{xz} = 0$. Since the nearest-neighbor ferromagnetic coupling J dominates, we anticipate all $\lambda \lesssim 1$.

Neutron scattering probes the DSF, which is related to the spin–spin correlation function of Hamiltonian $\mathcal{H}$ via

$$\mathcal{S}^{\alpha\beta}(\omega, k) \equiv \frac{1}{L} \int_{-\infty}^{\infty} dt \sum_{i,j} e^{ik(r_i - r_j)} e^{i\omega t} \langle S_i^\alpha(t) S_j^\beta \rangle, \qquad [5]$$

where $S_j^\alpha(t) = e^{i\mathcal{H}t} S_j^\alpha e^{-i\mathcal{H}t}$ and L is the total number of sites. For transverse (b-axis) field $h_y = 0$, operators $S_j^{x,y}$ excite a pair of DW excitations of the (Ising) ordered state. These are confined by a longitudinal (z-axis) mean field h_z. Of all of the symmetry-allowed nearest-neighbor exchange terms in ref. 4, only λ_{yz}, λ_A, and λ_{xy} produce DW hopping. We neglect the latter two terms in a first approximation as they create a DW continuum with double the k-space periodicity of that seen in experiments. This leads us to consider

$$\mathcal{H}_{dw} = J \sum_j \lambda_{yz} (-1)^j \left(S_j^z S_{j+1}^y + S_j^y S_{j+1}^z \right). \qquad [6]$$

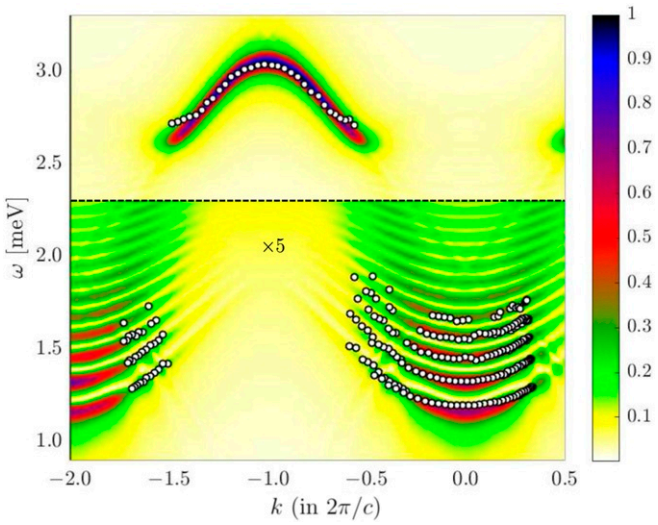

Fig. 2. DSF $\mathcal{S}^{xx}(\omega, k)$ at $h_y = 0$, scaled by a factor of 5 below the dashed line. Dots denote dispersion data points from the INS data of ref. 18. (tDMRG simulations truncated singular values $\lesssim \varepsilon = 2 \cdot 10^{-11}$ and used a Trotter step $\delta t = 2.5 \cdot 10^{-3}/J$ and broadening $\eta = J/125$ [*SI Appendix*].)

We have also verified that to $O(\lambda_{yz})$, the full Hamiltonian in Eq. **1** including $\mathcal{H}_{dw}$ reproduces the effective Hamiltonian for DW motion used to parametrize the $h_y = 0$ experimental data (12, 18). While $\mathcal{H} - \mathcal{H}_{dw}$ is symmetric under translation $T_{\tilde{c}}$: $r_j \mapsto r_j + \tilde{c}$ by a nearest-neighbor spacing $\tilde{c}$, $\mathcal{H}_{dw}$ only preserves translation T_c, with $c = 2\tilde{c}$. However, this unit cell doubling is invisible in the DSF, which is consistent with a BZ of size $2\pi/\tilde{c}$ (Fig. 2). Below, we link this to a nonsymmorphic glide symmetry $G \equiv T_{\tilde{c}} \circ \Sigma$, i.e., a translation by half a unit cell composed with a spin-flip $\Sigma = e^{i\pi \sum_j S^y_j}$ in the ab plane (consistent with the spatial reflection of a pseudovector spin). First, however, we determine the magnitude of the couplings in $\mathcal{H}$.

Numerical Results

We fix the parameters in $\mathcal{H}$ using exact diagonalization on small system sizes with $h_y = 0$. Through the fitting procedure described in *SI Appendix*, we find $J = 2.7607$ meV, $\lambda_{\mathrm{AF}} = 0.1507$, $\lambda_S = 0.2392$, $\lambda_{yz} = 0.1647$, and $J^{zz}_{\mathrm{ic}} = 0.0312$ meV. For the Hamiltonian thus obtained we compute the DSF for an effectively infinite system using tDMRG (*SI Appendix*). Our numerical results match the experimental data well (Fig. 2). We also compute the DSF in the high-field quantum paramagnetic regime, achieved for sufficiently strong transverse (i.e., b-axis) field. We set $h_z = 0$, consistent with the fact that the interchain mean field vanishes when $\langle S^z_j \rangle = 0$. To match simulations with data, we estimated $g_b \simeq 3.100$ by fitting the experimental dispersion at $B = 7$T (*SI Appendix*). A direct comparison of our results against data from ref. 20 (Fig. 3) shows excellent agreement, including features associated with quasiparticle breakdown—i.e., the apparent break in the dispersion of the QP band, traditionally understood as a decay of a QP as it enters the two-QP continuum, that occurs for sufficiently strong coupling (see, e.g., ref. 20). We now rationalize these results in terms of symmetries of $\mathcal{H}$.

Ising Criticality, Glide Symmetry, and BZ Unfolding

Hamiltonian Eq. **1** has neither translational symmetry by a nearest-neighbor spacing ($T_{\tilde{c}}$) nor on-site Ising symmetry (generated by Σ) as neither commutes with $\mathcal{H}_{dw}$. However, it preserves their product: glide symmetry G.

We now consider the unitary transformation $U = U^{-1} = e^{i\pi \sum_j S^y_{2j}}$, which reverses the Ising axis on alternate sites of the chain. It is straightforward to see that the invariance of $\tilde{\mathcal{H}} = U\mathcal{H}U^{-1}$ under $T_{\tilde{c}}$ is equivalent to that of $\mathcal{H}$ under G. The transformation flips the sign of the nearest-neighbor zz and xx couplings and staggers the h_z term, while leaving the h_y term unchanged. Crucially, $\tilde{\mathcal{H}}_{dw}$ is no longer staggered and hence preserves $T_{\tilde{c}}$ but continues to break global Ising symmetry $S^z_j \mapsto -S^z_j$. Thus, $\tilde{\mathcal{H}}$ describes a translationally invariant Ising antiferromagnet (AF) in a uniform transverse field h_y, with additional terms that break global Ising symmetry, augmented with a field h_z that couples to the AF order parameter field $m_s = \sum_j (-1)^j \langle S^z_j \rangle / L$. For $h_z = 0$, $\tilde{\mathcal{H}}$ continues to have a transition in the Ising universality class since the AF order parameter spontaneously breaks the lattice symmetry (21, 22) (see also ref. 23). Reversing the unitary transformation, we see that this corresponds to the spontaneous breaking of the glide symmetry of $\mathcal{H}$. In the ordered phase, $h_z \neq 0$ due to the interchain mean field and couples to the order parameter field m_s. Therefore, the near-critical ordered phase is described by the Ising CFT perturbed by the magnetization operator—precisely that for which E_8 symmetry-related bound states were predicted (7) and experimentally identified (18). Therefore, although our revised model Eq. **1** associates the Ising criticality of $CoNb_2O_6$ with the spontaneous breaking of glide symmetry rather than the on-site Ising symmetry, it remains consistent with previously reported experiments.

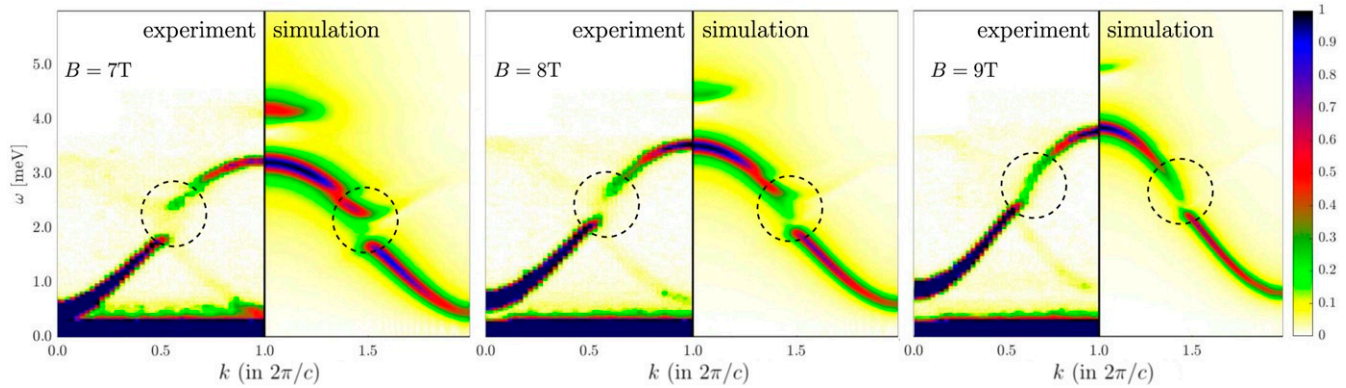

Fig. 3. Evolution of DSF in the polarized phase at large transverse field–as obtained from tDMRG simulations of $\mathcal{S}^{xx}(\omega, k)$ for the 1D Hamiltonian Eq. **1** (right image in each pair)–compared with inelastic neutron scattering data from ref. 21 (left image in each pair). Dashed circles indicate the regions of QP breakdown. (tDMRG parameters are $\delta t = 5 \cdot 10^{-3}/J$, $\varepsilon = 2 \cdot 10^{-10}$, $\chi_{max} = 400$, and $\eta = J/60$ [*SI Appendix*].)

The unitary transformation also allows us to view scattering experiments as probing the DSF of $\tilde{\mathcal{H}}$ (up to a k-space shift). To see this, observe that the DSF of $S^{\mu}_{k}=\sum_j e^{ikj\tilde{c}}S^{\mu}_{j}$ under the dynamics generated by $\mathcal{H}$ is equal to the DSF of $\tilde{S}^{\mu}_{k}=US^{\mu}_{k}U^{-1}$ under the dynamics generated by $\tilde{\mathcal{H}}$, as can be seen by inserting $U^{-1}U=\mathbb{1}$ in Eq. **5**. Either by studying the commutation relations of $\tilde{S}^{\mu}_{k}$ with $T_{\tilde{c}}$ or directly by inspecting $\tilde{S}^{\mu}_{k}=\sum_j e^{ikj\tilde{c}}US^{\mu}_{j}U^{-1}$, we see that S^{μ}_{k} changes the momentum as $\tilde{k}=k+\delta_{\mu}$ where $\delta_{x,z}=\pi/\tilde{c}$, and $\delta_{y}=0$. Consequently, since $\tilde{\mathcal{H}}$ has a unit cell of length $\tilde{c}$, the DSF will be $2\pi/\tilde{c}$-periodic as long as G is unbroken (i.e., in the high-field paramagnetic phase). In the ordered phase, where G is broken, we expect that the DSF is only $2\pi/c$-periodic (i.e., sees a smaller BZ). This is also corroborated by INS data (Fig. 4). Note, however, that exactly at $h_y=0$ we recover $2\pi/\tilde{c}$-periodicity of the DSF as evident in Fig. 2 since $\mathcal{H}$ has an extra glide symmetry given by $G'=T_{\tilde{c}}\circ e^{i\pi\sum_j S^{z}_{j}}$, which is explicitly broken for $h_y\neq 0$. (The same conclusions follow from the commutators of G with S^{μ}_{k}, as the operators G and $T_{\tilde{c}}$ are related by the unfolding U [*SI Appendix*].)

Note that rigorously speaking, this unfolding is possible only if different chains are decoupled. The presence of interchain couplings in the actual material means that the DSF will have small corrections not accounted for in our argument. However, we expect these corrections to be weak since the interchain couplings are two orders of magnitude weaker than the intrachain couplings (25), as can also be inferred from our estimate of J^{zz}_{ic}.

We now use this BZ unfolding perspective to interpret experiments on $CoNb_2O_6$. Scattering nonpolarized neutrons from a sample should yield superposition of the DSF of $\tilde{H}$ (from the y component) and the same DSF shifted in momentum k by $\pi/\tilde{c}$ (from the x and z components). However, in the high-field polarized phase, $\langle S^{y}_{j}\rangle$ is near saturation, thus largely suppressing the inelastic b component of the DSF. Hence, the dominant signal observed in this phase is the one at $k=\tilde{k}+\pi/\tilde{c}$; shifting the glide-labeled spectrum by $\pi/\tilde{c}$ thus reproduces the measurements. [A weaker-intensity shadow mode shifted by a wave vector $\pi/\tilde{c}$ visible in the experimental data is due to the fact that the scattering wave vector is not aligned with the c axis but has a nonzero component in the b direction, in addition to the component k along c (25) (*SI Appendix*). We note that alternative explanations of this mode that invoke interchain couplings can be ruled out due to the negligible magnitude of the latter.]

Quasiparticle Breakdown

The elementary excitations of the high-field phase are dressed spin-flips relative to the b-axis field. For $\lambda\neq 0$, these are interacting quasiparticles with rich physics. As seen in experiments and reproduced by our model (Fig. 3), they exhibit the striking feature of quasiparticle breakdown. Glide symmetry provides a natural resolution of why the decay of a single QP into the 2QP continuum that causes this effect is limited to a narrow, field-dependent range of momenta (Fig. 3). First, matching the k values with their respective $\tilde{k}$ as described above, we find that the minimum (maximum) of the single-QP dispersion $\omega_{\text{QP}}(\tilde{k})$ is at $\tilde{k}=\pi/\tilde{c}$ ($\tilde{k}=0$) as shown in Fig. 1. We stress that only $\tilde{k}$ is a good quantum number for $\mathcal{H}$, rather than the experimental wave vector k. With this in mind, the states that form part of the 2QP continuum in the $(\tilde{k},\omega)$ plane are those satisfying $\tilde{k}=\tilde{k}_1+\tilde{k}_2$, $\omega=\omega_{\text{QP}}(\tilde{k}_1)+\omega_{\text{QP}}(\tilde{k}_2)$. From this, we see that the entire upper section of the single-QP band is immersed in the continuum (Fig. 1*B*). We emphasize that this is sharply distinct (*SI Appendix*) from approaches that do not incorporate the glide symmetry and the corresponding $\pi/\tilde{c}$ momentum shifts (compare Fig. 1*B* to Fig. 2 and figure 6 of ref. 20).

Now, the QP-continuum matrix elements are at most $O(\lambda_{yz})$ as for $\lambda_{yz}=0$ the decay would be forbidden by $\mathbb{Z}_2$ (Ising) symmetry. Using Fermi's golden rule and neglecting to first approximation the dependence of matrix elements on momenta, the QP decay rate at wave vector k may be estimated as $\Gamma(k)\sim|\lambda_{yz}|^2\rho_2(\tilde{k},\omega(\tilde{k}))$. Here $\rho_2(\tilde{k},\omega)$ is the 2QP density of states (DoS), which is large (essentially an $(\omega-\omega_c(k))^{-1/2}$ singularity possibly renormalized by interactions) near the edges of the 2QP continuum (26–28). Hence, although in much of the 2QP continuum the decay rate is suppressed by $|\lambda_{yz}|^2\ll 1$, the large DoS near its edge allows full QP breakdown. This explains the relatively narrow region in momentum space where breakdown is visible in Fig. 3. In future high-resolution numerical and experimental studies, it may be interesting to probe the detailed transfer of spectral weight between the 1QP band and 2QP continuum for signatures of avoided quasiparticle decay (28).

Discussion

We have constructed a microscopic spin-exchange Hamiltonian to describe the 1D physics of $CoNb_2O_6$, based on a symmetry

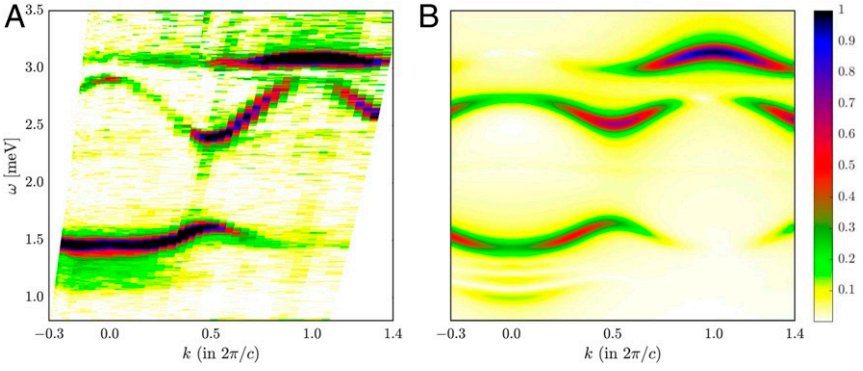

Fig. 4. (*A*) DSF measured by INS experiments in the ordered phased at intermediate transverse field (2.5 T) collected using the same experimental setup as in the field-dependent INS measurements reported in ref. 18. Sharp modes show the reduced periodicity of the structural $2\pi/c$ BZ, in contrast to the $4\pi/c$ periodicity in the ordered phase at zero field (Fig. 2) and the high-field paramagnetic phase (Fig. 3). This is tied to the breaking of glide symmetry G throughout the ordered phase except at $h_y=0$, which enjoys an extra glide symmetry G'. (*B*) DSF $S^{xx}(k,\omega)$ calculated via tDMRG ($\delta t=2.5\cdot 10^{-3}/J$, $\varepsilon=2\cdot 10^{-11}$, and $\eta=J/100$ [*SI Appendix*]). Key features of the spectrum in *A* including all dispersion shapes are qualitatively well reproduced, justifying the minimal Hamiltonian Eq. **1**. More precise quantitative agreement requires fitting data to the tDMRG simulations of Eq. **1** rather than a perturbative low-energy model (*SI Appendix*). This is very computationally demanding and beyond the scope of this work.

analysis of its 3D space group. We found quantitative agreement between simulations of the model and INS experiments in very different regimes, indicating that the proposed model realistically captures single-chain physics.

A crucial departure from previous studies lies in the symmetries of our model, which identifies a two-site unit cell and explicitly breaks the on-site Ising $\mathbb{Z}_2$ symmetry. However, it retains a glide symmetry inherited from the 3D space group. We showed through an explicit unfolding transformation that the glide symmetry leads to a larger BZ for INS than that expected from the size of the unit cell. This transformation also shows that the model is consistent with previous reports of Ising criticality in $CoNb_2O_6$, if the ordering is linked to the breaking of glide symmetry rather than on-site $\mathbb{Z}_2$.

From a more fundamental perspective, the model presented in this paper is a microscopic justification—based on the actual symmetries of the material—that a quantum critical phase transition with gap closing and reopening can exist in $CoNb_2O_6$. Experimentally, there are indeed abundant indications of a proximity to a 1D QCP in the Ising universality class in this material. However, gap closing has not yet been reported experimentally, and careful inspection of the crystal structure shows in fact that the material does not microscopically feature an exact purely magnetic Ising symmetry. Therefore, there is no a priori reason why the field-induced transition should be continuous and in the Ising universality class. Our work provides a clear answer to such questions: our model shows how the microscopic symmetries of $CoNb_2O_6$ admit a true QCP in the Ising universality class, with an order parameter that transforms under both magnetic and space-group symmetries.

Our work reveals how subtle aspects of crystal symmetry intertwine with the rich physics of quantum criticality and provides a unified picture of spontaneous ordering, confinement, and quasiparticle breakdown in a canonical Ising chain system. It raises further interesting questions as to how symmetry considerations impact the rich 3D phase structure of $CoNb_2O_6$ (2, 3, 5, 6, 29). Similar ideas are likely relevant to other chain [e.g., $BaCoV_2O_8$ (30, 31), $Sr_2V_2O_8$ (32), $SrDy_2O_4$ (33, 34), or azurite $Cu_3(CO_3)_2(OH)_2$ (35, 36)] and layer compounds with nonsymmorphic space groups (*SI Appendix*).

Materials and Methods

Fit of Parameters for $h_y = 0$. In order to fix the five parameters (J, λ_{AF}, λ_S, λ_{yz}, and J_{ic}^{zz}) of the Hamiltonian for $h_y = 0$, we resort to exact diagonalization on a small system of size $L = 14$. We checked that the dispersions of the two lowest confined bound states, unlike those of higher ones, are not strongly affected by finite size effects at $L = 14$. Furthermore, their dispersion can be quickly accessed by targeting the low-energy subspace using the Lanczos algorithm. We thus fitted parameters to minimize the square difference of the energy dispersion as obtained in two different ways: 1) experimentally, from INS (18), and 2) numerically, by interpolating exact-diagonalization results on an $L = 12$ site system, restricting our attention to the lowest two modes.

In order to avoid overfitting, we constrained the parameters to reproduce (at first order in perturbation theory) the dispersion of the kinetic mode as parametrized in ref. 18. This fixes

$$J\lambda_S = 0.6605 \text{ meV}, \quad [7]$$

$$(1-\lambda_{AF})J = 2.3447 \text{ meV}, \quad [8]$$

thus leaving only three free parameters to be fitted.

Details of the tDMRG Simulations. Working at $T = 0$, we computed the matrix-product state approximation of the ground state $|0\rangle$ of $\mathcal{H}$ on a chain of L sites using DMRG. From this, the state $|\psi\rangle = S^{\beta}_{L/2}|0\rangle$ can be computed. We then time-evolve the state, viz. $|\psi(t)\rangle = \exp(-iHt)|\psi\rangle$, through tDMRG, up to some maximum time t_{max}. The DSF can then be approximated by ref. 37.

$$S^{\alpha\beta}(\omega, k) = E\left[2\Re\left(\int_0^{t_{max}} dt \sum_i e^{ik(r_i - r_{L/2})} e^{i(\omega+\omega_0)t} \langle 0|S_i^{\alpha}|\psi(t)\rangle \mathcal{W}(t)\right)\right]. \quad [9]$$

Here we define $E[f](q) = f(q) + f(-q)$, which, exploiting the inversion symmetry about bond centers, is equivalent to averaging over the position of j. Finally, $\mathcal{W}(t)$ is a windowing function smoothly suppressing contributions at larger t, in such a way that the truncation at $t = t_{max}$ does not produce oscillations in the Fourier transform (this requires $\mathcal{W}(t_{max}) \ll 1$). In this paper, we use a Gaussian windowing $\mathcal{W}(t) \propto \exp\left[-(\eta t)^2/2\right]$ (38). Due to this choice the DSF obtained from the computation can be viewed as the convolution of the exact DSF with a Gaussian of width η, broadening spectral lines.

For a fixed broadening η, there are three parameters controlling the errors in the computation: the Trotter step δt in the time evolution, the singular value cutoff ε in the SVD, and a hard maximum χ_{max} of the maximum singular values we retain in the SVD. The values of these parameters are indicated in the caption of the corresponding figure. When χ_{max} is not explicitly reported, it is meant that a hard cutoff was unnecessary as the bond dimension growth was mild. Exact results are recovered as $\varepsilon \to 0$, $\chi \to \infty$, and $\delta t \to 0$. The convergence analysis for the results we report is presented in *SI Appendix*. Numerical simulations were performed using the ITensor Library (39).

Data Sharing. All numerical data of the theoretical calculations including all code used in the theoretical analysis and the experimental data points in Fig. 2 are available from the Oxford University Research Archive (40). The experimental data in Fig. 4*A* are available from the corresponding author on request. The experimental data in Figs. 2 and 3 are adapted/reproduced here from refs. 18 and 20.

ACKNOWLEDGMENTS. We thank Sarang Gopalakrishnan, Fabian Essler, Frank Pollmann, John Chalker, and Alexander Chernyshev for useful discussions. We also thank Ruben Verresen for useful comments on the manuscript. We acknowledge support from the European Research Council under the European Union Horizon 2020 Research and Innovation Programme via Grant Agreements 788814-EQFT (R.C.) and 804213-TMCS (S.A.P.).

1. A. Vasiliev, O. Volkova, E. Zvereva, M. Markina, Milestones of low-d quantum magnetism. *NPJ Quantum Mater.* **3**, 18 (2018).
2. S. Kobayashi, S. Mitsuda, M. Ishikawa, K. Miyatani, K. Kohn, Three-dimensional magnetic ordering in the quasi-one-dimensional Ising magnet $CoNb_2O_6$ with partially released geometrical frustration. *Phys. Rev. B* **60**, 3331–3345 (1999).
3. C. Heid *et al.*, Magnetic phase diagram of $CoNb_2O_6$: A neutron diffraction study. *J. Magn. Magn. Mater.* **151**, 123–131 (1995).
4. I. Maartense, I. Yaeger, B. Wanklyn, Field-induced magnetic transitions of $CoNb_2O_6$ in the ordered state. *Solid State Commun.* **21**, 93–96 (1977).
5. W. Scharf, H. Weitzel, I. Yaeger, I. Maartense, B. Wanklyn, Magnetic structures of $CoNb_2O_6$. *J. Magn. Magn. Mater.* **13**, 121–124 (1979).
6. S. Lee, R. K. Kaul, L. Balents, Interplay of quantum criticality and geometric frustration in columbite. *Nat. Phys.* **6**, 702–706 (2010).
7. A. B. Zamolodchikov, Integrals of motion and S-matrix of the (scaled) $T = T_c$ Ising model with magnetic field. *Int. J. Mod. Phys.* **4**, 4235–4248 (1989).
8. B. M. McCoy, T. T. Wu, Two-dimensional Ising field theory in a magnetic field: Breakup of the cut in the two-point function. *Phys. Rev. D* **18**, 1259–1267 (1978).
9. G. Delfino, G. Mussardo, P. Simonetti, Non-integrable quantum field theories as perturbations of certain integrable models. *Nucl. Phys. B* **473**, 469–508 (1996).
10. G. Delfino, G. Mussardo, The spin-spin correlation function in the two-dimensional Ising model in a magnetic field at $T = T_c$. *Nucl. Phys. B* **455**, 724–758 (1995).
11. P. Fonseca, A. Zamolodchikov, Ising spectroscopy I: Mesons at $T < T_c$ arXiv:hep–th/0612304 (29 December 2006).
12. J. A. Kjäll, F. Pollmann, J. E. Moore, Bound states and E_8 symmetry effects in perturbed quantum Ising chains. *Phys. Rev. B* **83**, 020407 (2011).
13. C. M. Morris *et al.*, Hierarchy of bound states in the one-dimensional ferromagnetic Ising chain $CoNb_2O_6$ investigated by high-resolution time-domain terahertz spectroscopy. *Phys. Rev. Lett.* **112**, 137403 (2014).
14. A. W. Kinross *et al.*, Evolution of quantum fluctuations near the quantum critical point of the transverse field Ising chain system $CoNb_2O_6$. *Phys. Rev. X* **4**, 031008 (2014).
15. T. Liang *et al.*, Heat capacity peak at the quantum critical point of the transverse Ising magnet $CoNb_2O_6$. *Nat. Commun.* **6**, 7611 (2015).
16. C. T. Bach, N. T. Nguyen, G. H. Bach, Thermodynamic properties of ferroics described by the transverse Ising model and their applications for $CoNb_2O_6$. *J. Magn. Magn. Mater.* **483**, 136–142 (2019).
17. S. Sachdev, *Quantum Phase Transitions* (Cambridge University Press, ed. 2, 2011).
18. R. Coldea *et al.*, Quantum criticality in an Ising chain: Experimental evidence for emergent E_8 symmetry. *Science* **327**, 177–180 (2010).

19. S. B. Rutkevich, On the weak confinement of kinks in the one-dimensional quantum ferromagnet $CoNb_2O_6$. *J. Stat. Mech. Theor. Exp.* **2010**, P07015 (2010).
20. N. J. Robinson, F. H. L. Essler, I. Cabrera, R. Coldea, Quasiparticle breakdown in the quasi-one-dimensional Ising ferromagnet $CoNb_2O_6$. *Phys. Rev. B* **90**, 174406 (2014).
21. S. Sachdev, K. Sengupta, S. M. Girvin, Mott insulators in strong electric fields. *Phys. Rev. B* **66**, 075128 (2002).
22. A. A. Ovchinnikov, D. V. Dmitriev, V. Y. Krivnov, V. O. Cheranovskii, Antiferromagnetic Ising chain in a mixed transverse and longitudinal magnetic field. *Phys. Rev. B* **68**, 214406 (2003).
23. M. A. Neto, J. R. de Sousa, Phase diagrams of the transverse Ising antiferromagnet in the presence of the longitudinal magnetic field. *Phys. A* **392**, 1–6 (2013).
24. C. P. Brock *et al.*, Eds., *International Tables for Crystallography*, M. Aroyo, Ed. (International Union of Crystallography, Chester, UK, 2016), Vol A.
25. I. Cabrera *et al.*, Excitations in the quantum paramagnetic phase of the quasi-one-dimensional ising magnet $CoNb_2O_6$ in a transverse field: Geometric frustration and quantum renormalization effects. *Phys. Rev. B* **90**, 014418 (2014).
26. B. Gaveau, L. S. Schulman, Limited quantum decay. *J. Phys. A. Math. Gen.* **28**, 7359–7374 (1995).
27. M. E. Zhitomirsky, A. L. Chernyshev, Colloquium: Spontaneous magnon decays. *Rev. Mod. Phys.* **85**, 219–242 (2013).
28. R. Verresen, R. Moessner, F. Pollmann, Avoided quasiparticle decay from strong quantum interactions. *Nat. Phys.* **15**, 750–753 (2019).
29. P. W. C. Sarvezuk *et al.*, New investigation of the magnetic structure of $CoNb_2O_6$ columbite. *J. Appl. Phys.* **109**, 07E160 (2011).
30. B. Grenier *et al.*, Longitudinal and transverse Zeeman ladders in the Ising-like chain antiferromagnet $BaCo_2V_2O_8$. *Phys. Rev. Lett.* **114**, 017201 (2015).
31. Q. Faure *et al.*, Topological quantum phase transition in the Ising-like antiferromagnetic spin chain $BaCo_2V_2O_8$. *Nat. Phys.* **14**, 716–722 (2018).
32. Z. Wang *et al.*, Spinon confinement in the one-dimensional Ising-like antiferromagnet $SrCo_2v_2O_8$. *Phys. Rev. B* **91**, 140404 (2015).
33. A. Fennell *et al.*, Evidence for $SrHo_2O_4$ and $SrDy_2O_4$ as model J_1-J_2 zigzag chain materials. *Phys. Rev. B* **89**, 224511 (2014).
34. C. Bidaud *et al.*, Dimensionality and irreversibility of field-induced transitions in $SrDy_2O_4$. *Phys. Rev. B* **93**, 060404 (2016).
35. K. C. Rule *et al.*, Magnetic and crystal structure of azurite Cu_3 $(CO_3)_2$ $(OH)_2$ as determined by neutron diffraction. *Phys. Rev. B* **83**, 104401 (2011).
36. H. Jeschke *et al.*, Multistep approach to microscopic models for frustrated quantum magnets: The case of the natural mineral azurite. *Phys. Rev. Lett.* **106**, 217201 (2011).
37. S. Paeckel *et al.*, Time-evolution methods for matrix-product states. *Ann. Phys.* **411**, 167998
(2019).
38. S. R. White, I. Affleck, Spectral function for the $s = 1$ Heisenberg antiferromagetic chain. *Phys. Rev. B* **77**, 134437 (2008).
39. M. Fishman, S. R. White, E. M. Stoudenmire, The ITensor Software Library for tensor network calculations. arXiv:2007.14822 (28 July 2020).
40. M. Fava, R. Coldea, S. A. Parameswaran, Data deposit at Oxford University Research Archive. https://dx.doi.org/10.5287/bodleian:Gw5vP7zJ7. Deposited 24 July 2020.